

Sodium bis(2-ethylhexyl)sulfosuccinate self-aggregation *in vacuo*: molecular dynamics simulation†

Giovanna Longhi,^{*ab} Sandro L. Fornili,^{bc} Vincenzo Turco Liveri,^d Sergio Abbate,^{ab} Davide Rebecani,^c Leopoldo Ceraulo^e and Fabrizio Gangemi^{‡a}

Received 17th November 2009, Accepted 25th February 2010

First published as an Advance Article on the web 18th March 2010

DOI: 10.1039/b924146a

Molecular dynamics (MD) simulations were conducted for systems *in vacuo* consisting of n AOT[−] anions (bis(2-ethylhexyl)sulfosuccinate ions) and $n \pm 1$ or n Na⁺ ions up to $n = 20$. For $n = 15$, positively charged systems with Li⁺, K⁺, and Cs⁺ cations were also considered. All systems were observed to form reverse micelle-like aggregates whose centre is occupied by cations and polar heads in a very compact solid-like way, while globally the aggregate has the form of an elongated and rather flat ellipsoid. Various types of statistical analyses were carried out on the systems to enlighten structural and dynamical properties including gyration radius, atomic pair correlation functions, atomic B-factor and moment of inertia tensor. For completeness and comparison the stability of reverse micelle is tested in the case of neutral $n = 20$ system in CCl₄ solution.

Introduction

Sodium bis(2-ethylhexyl)sulfosuccinate (AOTNa, see Fig. 1 for the anion structure and numbering of relevant atoms) is one of the few surfactants able to spontaneously form reverse micelles in apolar media without the addition of

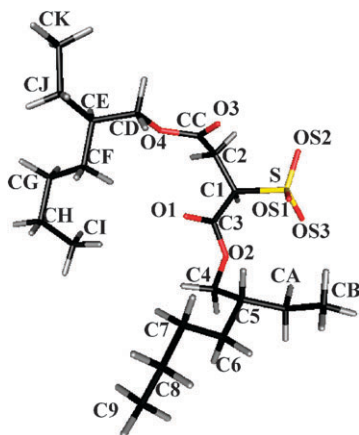


Fig. 1 Structure of the AOT[−] anion in the conformational minimum obtained by the *ab initio* calculation described in the text.

^a Dipartimento di Scienze Biomediche e Biotecnologie, Università di Brescia, Viale Europa 11, 25123 Brescia, Italy. E-mail: longhi@med.unibs.it

^b Consorzio Nazionale Interuniversitario per le Scienze Fisiche della Materia (CNISM), Via della Vasca Navale, 84 00146 Roma, Italy

^c Dipartimento di Tecnologie dell'Informazione and CISI, Università di Milano, via Bramante 65, 26013 Crema, Italy

^d Dipartimento di Chimica Fisica, Università di Palermo, Viale delle Scienze, Parco d'Orleans II, 90128 Palermo, Italy

^e Dipartimento di Chimica e Tecnologie Farmaceutiche, Università di Palermo, Via Archirafi 32, 90123 Palermo, Italy

† Electronic supplementary information (ESI) available: Net atomic charges, GAFF atomic types and geometric coordinates of the AOT[−] unit are available in mol2 format. See DOI: 10.1039/b924146a

‡ Present address: DIBIT, San Raffaele Scientific Institute, Via Olgettina 58, 20132 Milano, Italy.

cosurfactants.¹ The structural arrangement of these dynamical aggregates, attributed to the mutual interactions of spatially separated polar and apolar parts of AOTNa, is generally described in terms of a core formed by the hydrophilic headgroups and sodium counterions surrounded by the hydrocarbon tails protruding into the bulk apolar solvent. Although there is a broad consensus on this picture, no quantitative knowledge exists on the driving forces of the self-assembling process and on the structural and energetic details of these aggregates.

A wide variety of processes have been considered as responsible of the mechanism of aggregation, namely conformational movements of the hydrophilic and hydrophobic molecular moieties, micellar shape fluctuations, exchange of surfactant molecules between bulk solvent and micelle, diffusion and rotation of the whole aggregate and intermicellar collisions.^{2–5}

While structural and dynamical properties of AOTNa reverse micelles dispersed in apolar media have been extensively studied,^{1,5} only recently some experimental evidence on the formation of reverse micelle-like AOTNa aggregates in the gas phase has been reported.^{6,7} In particular, by electrospray ionization and energy-resolved mass spectrometry, the occurrence of a wide spectrum of AOTNa clusters has been observed, either as positive or negative ions, including those with an aggregation number close to that found in apolar media; additionally, marked differences in the mass distribution between negative and positive aggregates were reported. Surprisingly, the electrospray ionization process yields totally desolvated aggregates, suggesting that AOTNa–AOTNa interactions are stronger than water–AOTNa ones and that AOTNa–AOTNa mutual attractions are sufficient to stabilize charged aggregates. The addition of various alkali metal ions to the starting AOTNa solution has been also ascertained to lead to a wide range of aggregates where the sodium counterions are partially or totally replaced by the added cations. The stability and relative abundance of these aggregates resulted strongly influenced by the cation nature.⁷

To account for these experimental results, it was postulated⁷ that the main contributions to their structure and stability are intra-aggregate electrostatic interactions and screening of inter-aggregate interactions due to the excluded volume effect caused by the surfactant alkyl chains. However, while mass spectrometry is able to detect AOTNa self-assembling in the gas phase, it is unable to provide direct information on (i) the occurrence and stability of neutral aggregates, (ii) the structural arrangement of neutral and charged aggregates, (iii) the factors determining their architecture and (iv) the dynamical properties of aggregates. Concerning these points, we recognized that molecular dynamics simulations appear particularly suitable to gain such knowledge.

From a computational point of view, the geometries of several representative conformers of AOTNa have been analysed.⁸ Only minor effects on the postulated geometries are induced by the solvent, while their energies were found to be comprised in the range $-121/-131$ kcal mol⁻¹.

Further theoretical investigations were aimed at simulating the structural properties of water-containing AOTNa reverse micelles in apolar media, leaving the structural and dynamical features of “dry” AOTNa reverse micelles nearly unexplored.^{9,10} Another theoretical work concludes that the behaviour of water-containing reverse micelles formed by the poly(oxyethylene) surfactant, C₁₂E₂, *in vacuo* is similar to that in an apolar medium (decane).¹¹ Overall, the structure of the micelle core *in vacuo* is similar to the one in decane. However its exterior is different. In the absence of solvent, the tails collapse on the surface of the core, thus forming a more compact aggregate.

In the present report, the “dry” aggregates formed by AOTNa surfactant in the gas phase have been investigated by molecular dynamics (MD) simulations. A preliminary study of the role of the counterion nature and of carbon tetrachloride as micelle solvent has been also conducted. The latter system has been investigated for the main scope of evaluating the micelle density to be compared with experimental data. In the gas phase, simulations have been performed considering both neutral and charged aggregates, in order to unveil the role of an extra-charge on the aggregate stability. This investigation aims at finding reasonable explanations of the observed features in mass spectra, but may be useful also in view of their potential applications for drug transport and delivery in the gas phase. It may provide also clues for studying supramolecular aggregation in the interstellar space.¹²

From a more general point of view, we wish to stress that investigations of ordered surfactant self-assembly both *in vacuo* and in apolar solvent are of current interest to get some insight into the role played by the surfactant–surfactant interactions as the driving forces of the self-assembling mechanism in the absence of additional interactions due to surrounding solvent molecules as well as to unveil subtle effects caused by the solvent medium.

Computational methods

About ten conformations of the AOT⁻ anion, taken from a previous paper⁸ or generated by preliminary MD simulations using atomic charges given therewith and the all-atom General

Amber Force Field (GAFF),¹³ were optimized with GAUSSIAN-03¹⁴ at RHF/6-31G* level. These conformations have been then used to evaluate atomic charges suitable to AMBER force fields following the RESP protocol,¹⁵ as implemented in the Antechamber module of the AMBER 10 package.¹⁶ Furthermore, *ab initio* calculations for geometry optimization and electron charge density evaluations have been performed on the same conformations using the Onsager approach to mimic the presence of CCl₄. The ensuing RESP procedure to evaluate atomic charges yielded essentially the same AOT⁻ charge set as *in vacuo*. In the ESI† we present atomic charges, GAFF atomic types and geometric coordinates of the AOT⁻ R–R–R diastereoisomer (see Fig. 1), which has been chosen as building block both for *in vacuo* systems and for a CCl₄¹⁷ solution. All systems were constructed using the AMBER10 LeAP module which enables to choose the initial mutual orientation and distance of the AOT⁻ monomers, as well as their orientation and distance from the proper number of counterions and/or solvent molecules. Simulations were carried out at $T = 300$ K using the parallel version of the AMBER10 SANDER module with a time-step of 2 fs. SHAKE¹⁸ was used to keep constrained the bonds involving hydrogen atoms. For *in vacuo* simulations, the system temperature was controlled according to the Berendsen coupling algorithm (with a time constant of 0.5 ps), and a 999 Å cutoff was applied for non-bonded interactions. The equilibration phase of each simulation *in vacuo* was carried out according to the following protocol: in the first 1 ns time interval, the AOT_{*x*}Na_{*y*} self-aggregation at 300 K was favoured by restraining the AOT–AOT intermolecular distance to within 40 Å by a flat-well function (*i.e.*, no restraining force was applied until the distance between every two AOT⁻ anions is less than 40 Å, whereas a restraining parabolic potential is switched on at that distance with a constant of 30 kcal mol⁻¹ Å⁻²). This was found necessary for some aggregation numbers, since the absence of a box and the arbitrarily chosen and rather loose initial conformations made it difficult to end up this first step with a single aggregate. In all the following phases the restraining force was switched off and the aggregates did not break, even at high temperature. Indeed, the system temperature was gradually increased up to 700 K during 1 ns time interval, so that it loses memory of its original conformation and its evolution is speeded up. Thereafter the system temperature was brought back to 300 K by evenly decreasing it in one hundred 40-ps steps, during which the temperature was kept constant.

The systems considered in the present work for *in vacuo* simulation consist of *n* AOT⁻ anions, for the cases $n = 1-7, 10, 15$ and 20. In all instances we have included the proper number of Na⁺ ions to make the overall system either negative [AOT_{*n*}Na_{*n-1*}]⁻, or neutral [AOT_{*n*}Na_{*n*}] or positive [AOT_{*n*}Na_{*n+1*}]⁺. For the $n = 15$ case, we have also simulated systems obtained by replacing Na⁺ with Li⁺, K⁺ and Cs⁺ ions. The production phase of each MD simulation *in vacuo* was 50 ns long.

In addition we have conducted a NPT simulation ($T = 300$ K, $p = 1$ bar) of a neutral system in CCl₄ consisting of 20 AOT⁻ and Na⁺ ions. For this system a 15 Å cutoff, PME (Particle Mesh Ewald) and the Langevin dynamics with $\gamma = 2$ ps were

used. Its initial conformation was built starting from the last conformation of the corresponding simulation *in vacuo*. This “solute” was immersed into a truncated octahedral box, surrounded by 810 CCl₄ molecules. The latter number results from requiring that the minimum distance between solute atoms and box surface be 15 Å. The total length of the production phase of the MD simulation in CCl₄ was 100 ns. Truncated octahedral periodic boundary conditions were assumed during the simulation of this system.

The statistical analysis of the trajectories was mainly based on the PTRAJ module of the AMBER 10 package, while the Voronoi volume evaluation was carried out as outlined in ref. 19, and the moments of inertia were calculated as described in ref. 20. Graphical analysis was performed using VMD,²¹ gOpenMol²² and Rasmol.²³

Results and discussion

In Fig. 2 we report the total potential energy values E for [AOT_{*n*}Na_{*x*}] systems *in vacuo* as a function of the surfactant aggregation number n , for the three situations described above, namely the negatively charged [AOT_{*n*}Na_{*n-1*}]⁻, the neutral [AOT_{*n*}Na_{*n*}] and the positively charged [AOT_{*n*}Na_{*n+1*}]⁺ systems. The linear decrease indicates that, within the examined range of aggregation number, each AOTNa molecule added to the cluster contributes the same amount of stabilization energy. From this figure, one sees that, quite independently on n , the positively charged aggregates are more stable than the neutral ones (of about 75 kcal mol⁻¹ of aggregates) and that the latter are more stable than the negatively charged systems (of about 135 kcal mol⁻¹ of aggregates), in qualitative

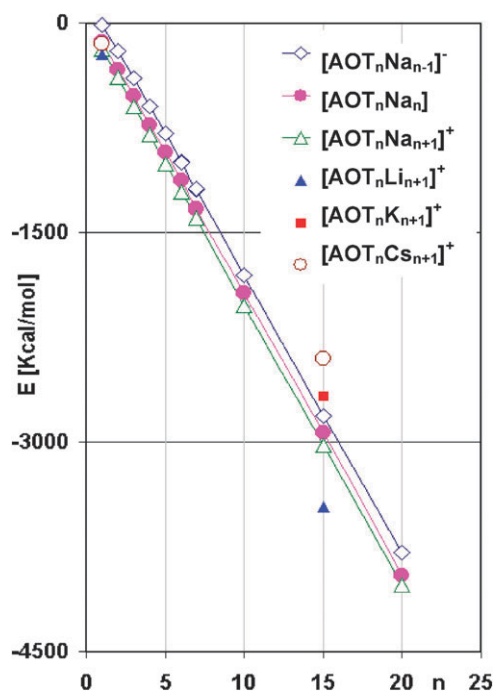


Fig. 2 Plot of calculated potential energy values (units of kcal mol⁻¹ of aggregates) versus the aggregation number n for [AOT_{*n*}Na_{*n-1*}]⁻, [AOT_{*n*}Na_{*n*}] and [AOT_{*n*}Na_{*n+1*}]⁺ systems, and for [AOT₁₅Li₁₆]⁺, [AOT₁₅K₁₆]⁺ and [AOT₁₅Cs₁₆]⁺ systems.

agreement with experimental observations on charged clusters.^{6,7} Such experiments cannot be performed for neutral aggregates but a behaviour intermediate between positively and negatively charged aggregates is expected. Furthermore, we observe that the nature of counterions, namely Li⁺, K⁺, and Cs⁺ (examined for the case $n = 15$), affects appreciably the aggregation energy value E , which increases as the ion dimension decreases. This behavior is observed to be in qualitative agreement with the experimental collision energies in the center-of-mass reference frame obtained by energy-resolved mass spectra.⁷ In particular, the collision energies required to dissociate 50% of the positively charged trimers AOT₃Li₄⁺, AOT₃Na₄⁺ and AOT₃Cs₄⁺ leading to the formation of charged dimers and neutral monomers are 0.0049 eV, 0.0047 eV and 0.0022 eV, respectively.

To monitor the aggregation mechanism, we have studied the time dependence of the mass weighted gyration radius R_G , defined as:

$$R_G = \sqrt{\frac{\sum_{i=1}^N m_i (\mathbf{r}_i - \mathbf{R})^2}{\sum_{i=1}^N m_i}}$$

where \mathbf{R} represents the position vector of the centre of mass. The sum has been extended to all atoms (total R_G) or to just the core atoms, namely the cations and the sulfur and oxygen atoms of the SO₃⁻ group (core R_G); mass weighting has been performed accordingly. We report in Fig. 3 an example of the time evolution of R_G for the neutral system [AOT₁₅Na₁₅]. Reaching the reverse micelle equilibrium condition is quite fast indeed, despite the fact that the very first initial geometry consists of well separated AOT Na units, giving a total R_G value of 22.35 Å and a core R_G value of 19.41 Å. The systems equilibrate to a definite R_G value during the thermal treatment described in the Computational Methods section and reported in Fig. 3 for negative time values. R_G then maintains approximately this value during the subsequent simulation. From Fig. 3 we infer that the thermal treatment provides the AOT⁻ polar heads and their counterions with the required mobility that allows them to meet each other and allows the AOT⁻ backbone to disorder conformationally: more specifically, one may observe that

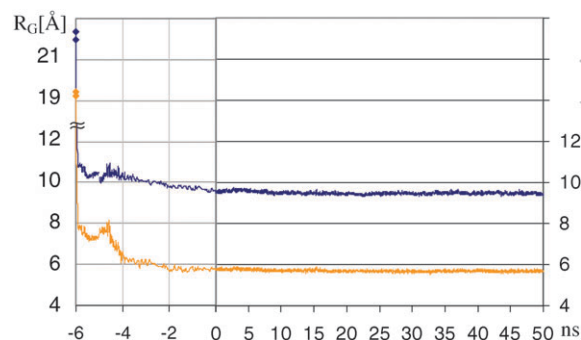


Fig. 3 Plot of the time evolution of the gyration radius R_G (Å) for the system [AOT₁₅Na₁₆]⁺. The self-aggregation phase at 300 K (1 ns time interval) and the thermal treatment phase (1 ns time interval with temperature increasing and 4 ns time interval decreasing temperature as described in the text) are reported on a more expanded negative time scale. The production phase corresponds to positive time values.

Table 1 Geometrical characteristics of the simulated $[\text{AOT}_n\text{Na}_{n-1}]^-$, $[\text{AOT}_n\text{Na}_n]$ and $[\text{AOT}_n\text{Na}_{n+1}]^+$ systems, of $[\text{AOT}_{15}\text{Li}_{16}]^+$, $[\text{AOT}_{15}\text{K}_{16}]^+$, and $[\text{AOT}_{15}\text{Cs}_{16}]^+$ systems *in vacuo*. The last row is for $[\text{AOT}_{20}\text{Na}_{20}]$ system in CCl_4 solution

	Total $R_G/\text{\AA}$	Core $R_G/\text{\AA}$	Total e	Total e'	Core e	Core e'
$[\text{AOT}_5\text{Na}_4]$	6.9	3.7	0.70	0.59	0.92	0.69
$[\text{AOT}_5\text{Na}_5]^+$	6.8	3.5	0.65	0.53	0.89	0.73
$[\text{AOT}_5\text{Na}_6]^+$	6.8	3.4	0.68	0.46	0.82	0.42
$[\text{AOT}_{10}\text{Na}_9]^-$	8.4	4.8	0.67	0.38	0.90	0.71
$[\text{AOT}_{10}\text{Na}_{10}]$	8.2	4.4	0.49	0.33	0.80	0.73
$[\text{AOT}_{10}\text{Na}_{11}]^+$	8.3	4.5	0.59	0.36	0.87	0.69
$[\text{AOT}_{15}\text{Na}_{14}]^-$	9.6	5.8	0.69	0.42	0.91	0.74
$[\text{AOT}_{15}\text{Na}_{15}]$	9.5	5.7	0.65	0.43	0.86	0.55
$[\text{AOT}_{15}\text{Na}_{16}]^+$	9.8	6.3	0.76	0.40	0.93	0.61
$[\text{AOT}_{15}\text{Li}_{16}]^+$	10.2	6.5	0.85	0.59	0.95	0.75
$[\text{AOT}_{15}\text{K}_{16}]^+$	10.1	6.9	0.80	0.46	0.95	0.72
$[\text{AOT}_{15}\text{Cs}_{16}]^+$	9.6	6.7	0.72	0.53	0.89	0.73
$[\text{AOT}_{20}\text{Na}_{19}]^-$	11.6	8.5	0.86	0.43	0.96	0.61
$[\text{AOT}_{20}\text{Na}_{20}]$	10.8	7.0	0.81	0.61	0.96	0.91
$[\text{AOT}_{20}\text{Na}_{21}]^+$	11.1	7.9	0.83	0.47	0.96	0.59
$[\text{AOT}_{20}\text{Na}_{20}] : \text{CCl}_4$	11.5	7.8	0.85	0.52	0.97	0.78

the core R_G starts decreasing during the heating phase (reported at times lower than -4 ns) and reaches equilibrium faster than the total R_G , which increases during the heating phase and decreases thereafter. In Table 1 we provide the geometrical characteristics of the formed micelles, in particular the average R_G values for all examined systems. From this table one may notice that total and core R_G values are smaller for neutral clusters than for charged clusters, as a possible consequence of an additional repulsive effect due to the presence of extra charge.

In Fig. 4 we provide snapshots of the conformation of the $n = 15$ positively charged systems, with the four ion types, at $t = 50$ ns. One gets a vivid picture that reverse micelle-like aggregates are formed: the presence of positive counterions in the centre of the micelle allows the repulsive interaction of negatively charged surfactant polar heads to be overcome. We notice that slightly different shapes are associated with different types of counterions: indeed the overall micelle shape is more spherical for Cs^+ case than for the other cations, while for Li^+ is somewhat bent.

A deeper analysis of the micellar structure allows one to distinguish a core, in which Coulomb interactions play the major role, and an external layer consisting of alkyl chains. This layered structure is illustrated in Fig. 5, where we report the average distance d of a few relevant atoms from the micelle centre of mass (for atoms' nomenclature see Fig. 1). As expected, the average distances increase with the aggregation number n , showing just little differences between differently charged aggregates. However this figure does not evidence the actual shape of the core and of the micelle as a whole.

For this reason we analysed the three principal moments of inertia I_1 , I_2 and I_3 of all the simulated micelles, obtained by evaluating the eigenvalues of the inertia tensor (see for example ref. 20). We report in Fig. 6 their time averaged values, which obviously increase with n ; the plot also suggests that, especially for $n = 15$ and $n = 20$ aggregates, one obtains $I_1 \ll I_2 < I_3$. From I_1 , I_2 and I_3 one may construct an equivalent homogeneous ellipsoid in the three dimensional geometrical space with principal semiaxes a , b

and c ($a \gg b > c$) having the same three moments of inertia. Semiaxis lengths are given by:

$$a^2 = \left(\frac{5}{2M_{\text{tot}}}\right)(I_1 + I_2 + I_3 - 2I_1)$$

$$b^2 = \left(\frac{5}{2M_{\text{tot}}}\right)(I_1 + I_2 + I_3 - 2I_2)$$

$$c^2 = \left(\frac{5}{2M_{\text{tot}}}\right)(I_1 + I_2 + I_3 - 2I_3)$$

where M_{tot} is the total mass; a is always assumed to be the largest semiaxis length. This permits to express the eccentricity parameter e related to a and c semiaxes and the eccentricity e' related to b and c . Following ref. 24, they are defined as:

$$e = \sqrt{1 - \left(\frac{c^2}{a^2}\right)} \quad e' = \sqrt{1 - \left(\frac{c^2}{b^2}\right)}$$

In Table 1 we report the eccentricities e and e' evaluated for the micelles and for the polar heads. From these values we have the clear picture that the micelle has the form of an elongated fairly flat ellipsoid and that the core is highly eccentric also at low aggregation number.

We have also examined how regularly the polar heads are assembled: in Fig. 7 we report the position of C1 carbon atoms, S atoms and cations with respect to the principal axes a , b and c as observed in the last 2.5 ns of the MD simulations. The plots give projections of the micellar core onto the three planes defined by the three couples of axes (a, b) , (a, c) , and (b, c) and show that the examined atoms are organized in nearly fixed positions. Since C1 is at the origin of the two aliphatic tails of AOTNa (see Fig. 1) and it is a stereogenic carbon of R absolute configuration in the case chosen here, a global handedness for the system might occur. However, considering a direction tangent to the ellipse in the plane b, c of Fig. 7 (lowest row) and oriented clockwise around the positive a axis we could not establish any chiral organization of the orientation of the two aliphatic tails.

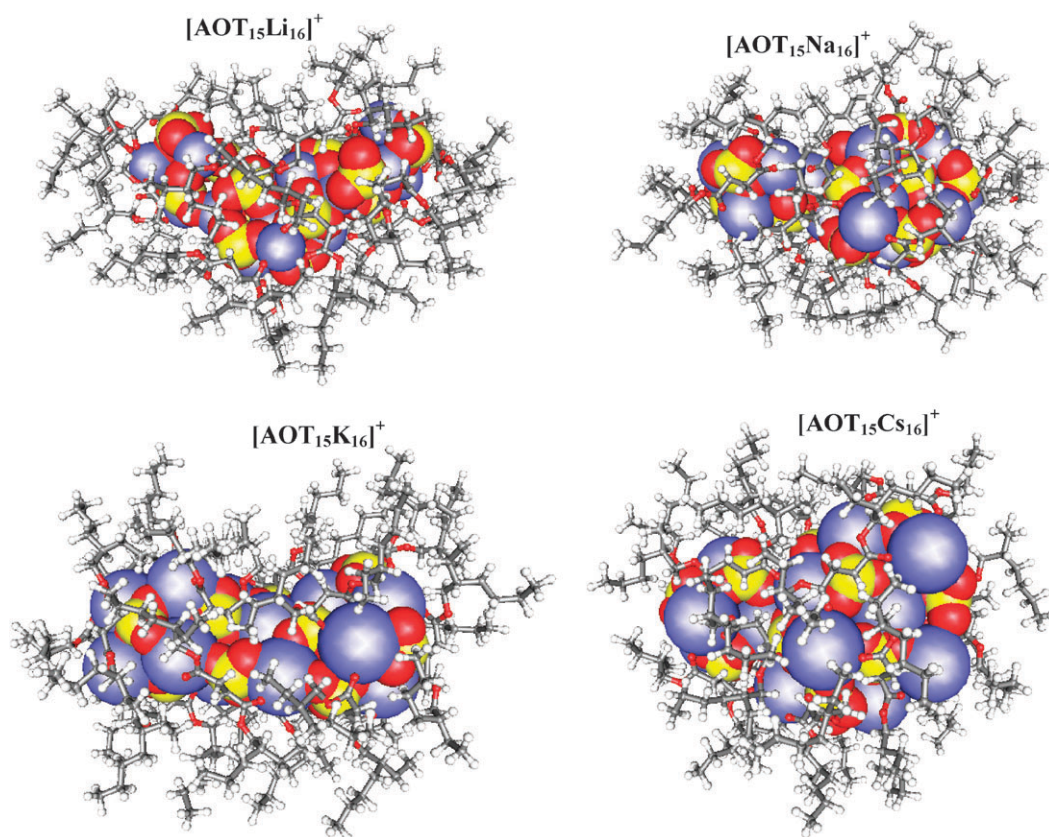


Fig. 4 Conformation of the $[\text{AOT}_{15}\text{Li}_{16}]^+$, $[\text{AOT}_{15}\text{Na}_{16}]^+$, $[\text{AOT}_{15}\text{K}_{16}]^+$ and $[\text{AOT}_{15}\text{Cs}_{16}]^+$ systems as obtained by the MD simulation at $t = 50$ ns. Cations (blue) and SO_3^- polar heads (red oxygen atoms and yellow sulfur atoms) are displayed in a space-filling mode to evidence structural properties of the micelle centres.

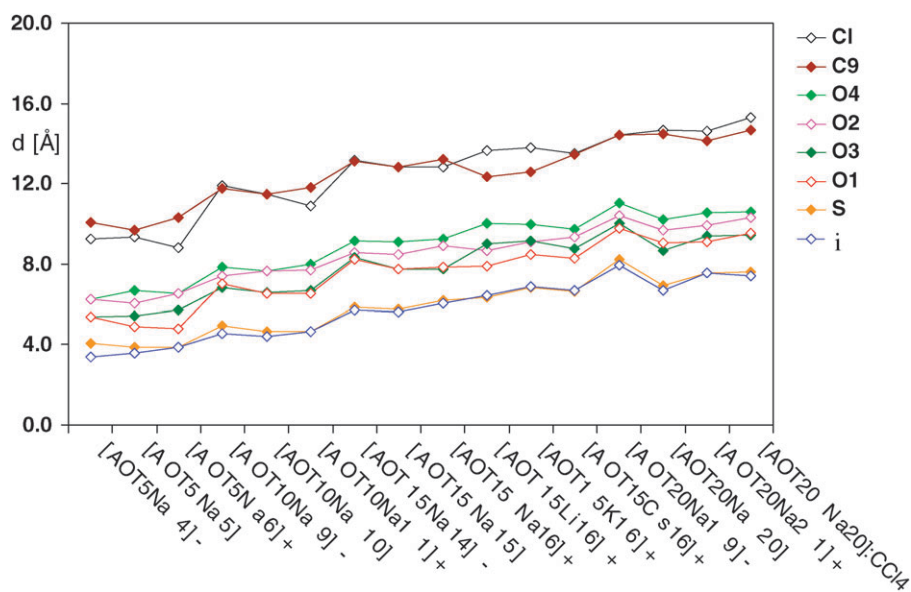


Fig. 5 Average distance d (Å) of selected atoms from the centre of mass of the simulated micelle systems. The atom labels are as in Fig. 1 and “i” represents cations; for the nomenclature of the micelle in the abscissa axis see text. The average is over all the homonymous atoms in the cluster, time average over the last 10 ns.

To get further insight about the packing inside the micellar core we have computed pair correlation functions, $g(r)$,¹⁸ for selected ion–atom pairs and report them in Fig. 8. From the

observed height and sharpness of the first $g(r)$ peak, which is found at a quite small distance in the case of the three pairs cation–OS, cation–O1, cation–O3, we get a further evidence of

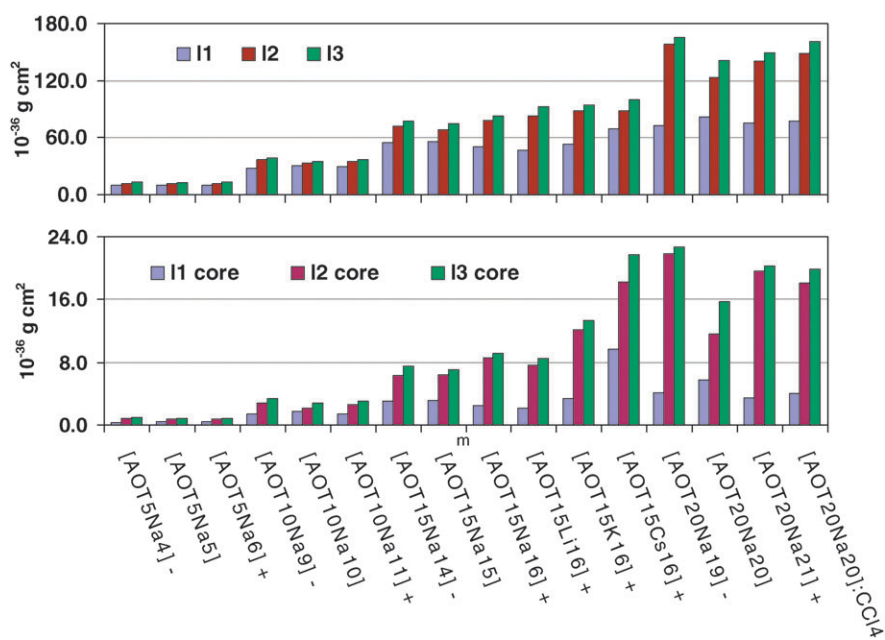


Fig. 6 Upper: average values (over a time period $\Delta t = 50$ ns) of the three principal moments of inertia (in 10^{-36} g cm^2), for *in vacuo* systems and for the CCl_4 solution. (See text for notation.) Lower: average values of principal moments of inertia evaluated for micelle core, namely counterions and SO_3^- groups.

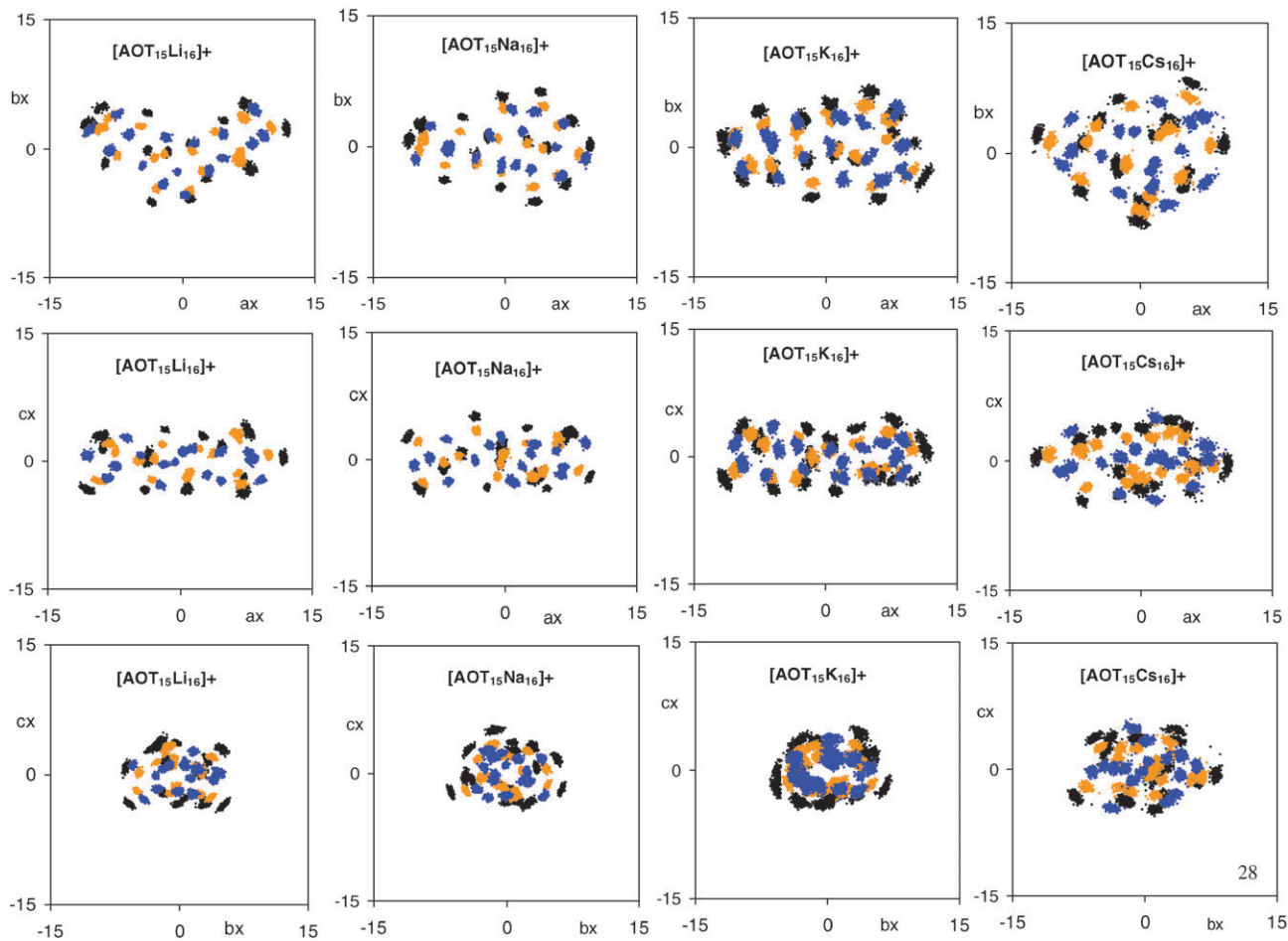


Fig. 7 Projections of the positions occupied by atoms Cl (black), S (orange) and ions (blue) in the last 2.5 ns of the simulations onto the planes (a, b), (a, c), and (b, c) passing through the centre of mass of the following systems: $[\text{AOT}_{15}\text{Li}_{16}]^+$, $[\text{AOT}_{15}\text{Na}_{16}]^+$, $[\text{AOT}_{15}\text{K}_{16}]^+$, $[\text{AOT}_{15}\text{Cs}_{16}]^+$ *in vacuo*. a, b, c are the principal axes of inertia of the equivalent homogeneous ellipsoid.

how tightly packed the micelle core is. This is characteristic of a solid-like structure, as if the AOTNa molecules were

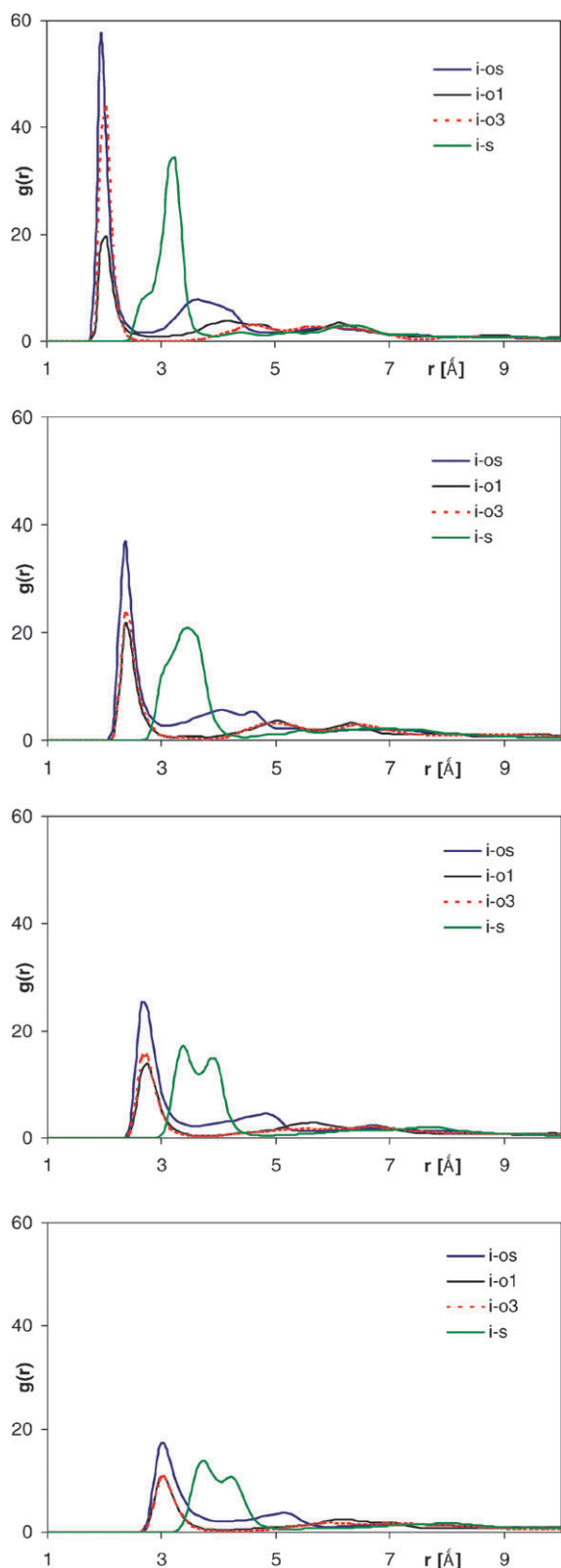


Fig. 8 Pair correlation functions, $g(r)$, for the i-OS, i-O1, i-O3, i-S pairs, where i indicates the cation (see Fig. 1 for the atoms labels) in the $[\text{AOT}_{15}\text{X}_{16}]^+$ ($\text{X} = \text{Li}, \text{Na}, \text{K}, \text{Cs}$) systems. The i-OS data are averaged over the $g(r)$ obtained for the three pairs i-OS1, i-OS2 and i-OS3.

Table 2 Distance, r_{\min} (in Å), of the first minimum of the $g(r)$ for cation-S atom pairs and average number, $N(r_{\min})$, of S atoms surrounding one cation within that distance for all the positively charged systems corresponding to the aggregation number $n = 15$

	r_{\min}	$N(r_{\min})$
Li+	3.85	3.5
Na+	4.45	4.0
K+	4.65	3.9
Cs+	5.15	3.9

anchored to a core that looks like an ionic solid. It is also interesting to notice that, especially for the Li^+ case and, to a lesser extent, for the Na^+ case, there is some difference in the behavior of the O1 and O3 correlation functions to the micelle-counterions. The i-S pair correlation function exhibits the first peak at larger distance than the previously mentioned correlation functions: this first peak is split and the ratio of the two components is progressively inverted in going from the Li^+ to the Cs^+ case. We attribute this different behavior to the ion size, allowing the smallest ion to get very close to one S atom at a time, while the largest ion can be very close to more than one atom S at a time. We report in Table 2 the average number of S nearest neighbours surrounding one cation as calculated by integrating the $g_{i-S}(r)$ up to the ion-sulfur distance corresponding to the first $g(r)$ minimum, r_{\min} .

To get some insight into the dynamics of the atoms within the aggregate we provide in Fig. 9 the atomic B-factor, which represents the average positional fluctuations of the individual atoms represented in Fig. 1. That is to say, we construct the B-factor by averaging over time and over the homologous atoms within the surfactant molecules of the cluster of the usual B-factor defined as follows:

$$BF_i(t) = \frac{8\pi^2}{3} \langle |\mathbf{u}_i(t)|^2 \rangle$$

where $\mathbf{u}_i(t)$ is the displacement of atom i at time t , averaged over 10 ps time intervals.²⁰ In the figure we report the results for all heavy atoms. From these data one may notice that the core atoms look indeed rather motionless with a behavior reminiscent of atoms in a solid, showing a B-factor of 2–6 Å² (smaller for ions, carbonyl oxygens and oxygens of SO_3^- groups, larger for the other oxygen atoms). Furthermore, in all examined cases, the atomic B-factor values are larger for the negatively charged clusters than for the positive and neutral ones, paralleling the energy behavior previously described (see Fig. 2). The B-factor of course increases for carbon atoms along the aliphatic chains, reaching values that are one order of magnitude larger for the end-chain methyl groups. For the carbon atoms of the two end-methyl groups the B-factors are similar (being larger for C9, which belongs to the longer chain in the case of low aggregation number) and decrease as the aggregation number increases since the packing of the aliphatic chains hinders atomic displacements. For the sake of comparison we show the same B-factor plot for the $\text{AOT}_{20}\text{Na}_{20}$ solution in CCl_4 . It is evident that the atom positional fluctuations are strongly attenuated by the solvent for the alkyl chains, as expected, leaving the behaviour of the micelle core unaltered.

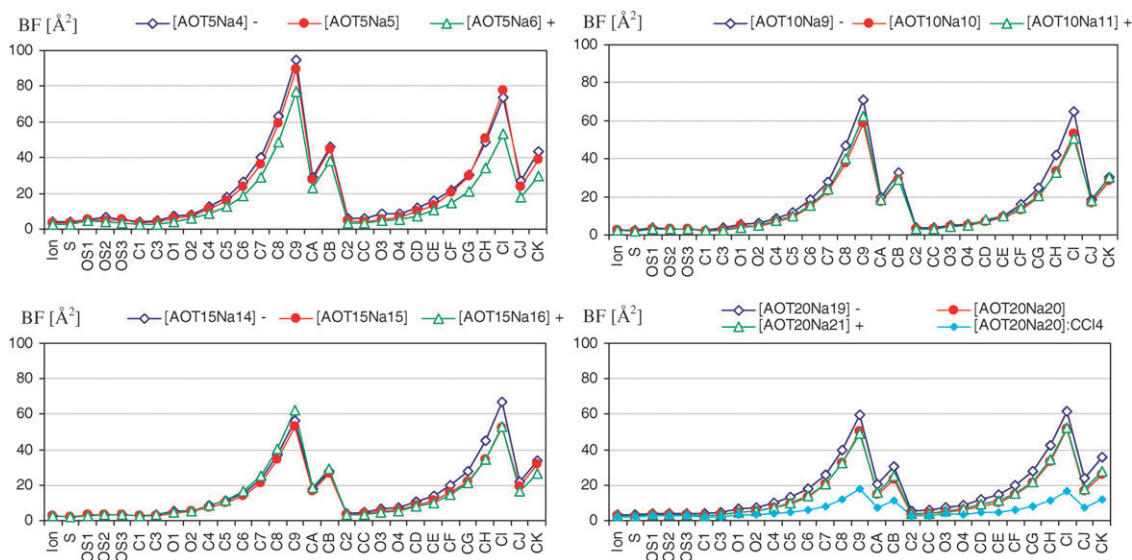


Fig. 9 Average B-factor (\AA^2) for all the atoms indicated in Fig. 1 for $[\text{AOT}_n\text{Na}_{n-1}]^-$ systems, for $[\text{AOT}_n\text{Na}_n]$ systems and for $[\text{AOT}_n\text{Na}_{n+1}]^+$ systems ($n = 5, 10, 15,$ and 20) *in vacuo*, and for the neutral system with $n = 20$ in CCl_4 solution.

With the aim of examining the spatial mobility/readjustment of the atoms within the micelles *in vacuo*, we monitored the mean square displacement, $\langle |r_i(t)|^2 \rangle$, of Na^+ ions, of SO_3^- groups and of the four terminal carbons of the alkyl chains. They were evaluated along the last 20 1-ns trajectory segments. Their average is reported in Fig. 10 for a representative case, since all the systems show a very similar behavior. We observe that these displacements are very small; for this reason a real diffusion of the ions inside the micelle can be excluded. It is reasonable to approximate $\langle |r_i(t)|^2 \rangle$ with a t^α power law, as in the cases of confined diffusion reported in the literature.^{9,25} We provide in Table 3 the α values, which in the case of Na^+ and SO_3^- decrease with increasing aggregation number n , reaching an approximately constant value after $n = 10$. On the contrary, the exponent α is almost constant for the terminal C atoms. Since the differences of α values corresponding to different aggregate charges are within the computational error, we report in Table 3 only their average value.

Another interesting geometrical property to be evaluated is a physically reasonable measure of the volume to be attributed to the micelle, which properly takes into account the excluded volume of the aliphatic tails. For this reason we have first calculated the Voronoi's volume¹⁹ for the micelle dissolved in CCl_4 . In this way we obtained a micelle density in CCl_4 of about 1.2 g cm^{-3} , which is in accordance with experimental data.²⁶ The treatment we adopted follows the statement of Marchi *et al.*⁹ that the "effective" volume of the micelle is due to a compact inner core plus a hairy highly fluctuating part, which does not simply occupy the whole sphere from the centre to the outermost atoms of the longer aliphatic arm of each AOTNa molecule. Although the present simulation of the $\text{AOT}_{20}\text{Na}_{20}$ system is preliminary, its analysis shows that the characteristics of the micelles in CCl_4 are quite similar to those for micelles *in vacuo*. Differently from what was observed in the case of MD simulations of polyoxyethylene *in vacuo* and in decane,¹¹ for AOTNa micelles the external

aliphatic layer behaves quite similarly in empty space and in CCl_4 solution: the AOTNa molecule has a sort of cone-shape with its two branched, relatively short, alkyl chains and their entanglement is such that they cannot collapse. This feature induces similar results for R_G and shape (Table 1), and for distances of the various atoms from the micelle centre (Fig. 4).

Conclusions

In this work we have investigated by MD simulations structural and dynamic properties of positively and negatively charged as well as of neutral AOTNa self-assembled aggregates *in vacuo* at various aggregation numbers. The main conclusions that can be drawn are the following.

(1) The aggregates are invariably characterized by a reverse micelle-like structure. They are stable even without water. This is remarkable since usually in MD simulations of systems dissolved in apolar solvent a percentage of water is considered;⁹ however in the gas-phase experiments no trace of water has been observed by mass spectroscopy also in cases where the starting solution was not anhydrous.⁷

(2) The aggregation number being equal, the positively charged micelles in the gas phase are more stable than the corresponding negatively charged ones, in qualitative agreement with the experimental results. Moreover, by replacing sodium ion with Li^+ , K^+ , or Cs^+ ion, the aggregation energy value increases as the dimension of the ion-type decreases, again in qualitative agreement with experimental observation.

(3) Neutral micelles, for which electrospray ionization and energy-resolved mass spectrometry experimental results are not available in the gas phase, show intermediate stability between positively and negatively charged micelles.

(4) Statistical structural analyses show that the micelles have the shape of elongated rather than flat ellipsoids, for which we evaluated the eccentricity parameters.

(5) Pair correlation function, $g(r)$, and B-factor analyses show that the micelle core composed by the surfactant and

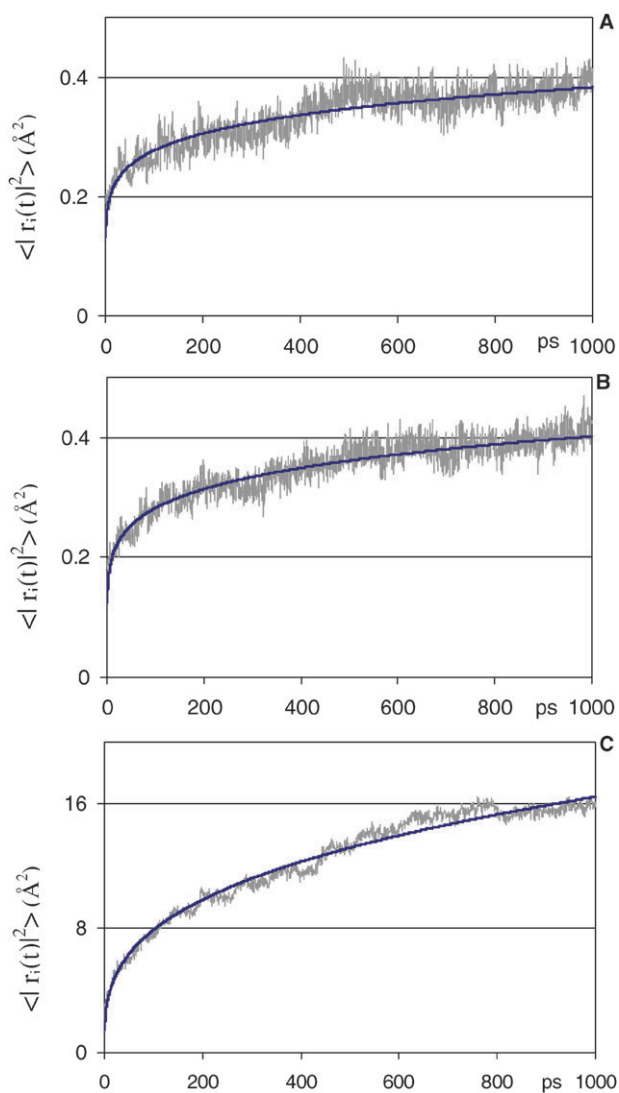


Fig. 10 Plot of the mean square displacement $\langle |r_i(t)|^2 \rangle$ values versus time of Na^+ ions (panel A), SO_3^- groups (panel B) and terminal carbon atoms of the branched aliphatic chains (panel C) for the case [AOT]₁₅Na₁₆.

Table 3 α constants for the fitting t^α to $\langle |r_i(t)|^2 \rangle$ data for [AOT]_nNa_{n+x}] ($x = 0, +1, -1$) for Na^+ ions, SO_3^- groups and alkyl chains terminal C atoms (see Fig. 10 and text)

n	Na^+	SO_3^-	C term
3	0.40	0.41	0.32
5	0.35	0.35	0.35
7	0.29	0.31	0.32
10	0.17	0.20	0.31
15	0.14	0.16	0.29
20	0.15	0.15	0.29

comprised of anionic polar heads and positive counterions possesses a solid-like structure and dynamics, while the more external the CH_2 groups of the alkyl chains are, the higher mobility they possess.

(6) The Voronoi volume for a neutral reverse micelle of AOT₂₀Na₂₀ in CCl_4 is in reasonable agreement with experimental data obtained by density measurements on similar

systems. This lends plausibility to our AOT model which is based on Amber GAFF force field.

Acknowledgements

Financial support from MIUR 60%, PRIN 2006 and Fondazione Cariplo is gratefully acknowledged.

References

- P. L. Luisi, L. J. Magid and J. H. Fendler, *CRC Crit. Rev. Biochem.*, 1986, **20**, 409–474.
- P. D. Fletcher and B. H. Robinson, *Ber. Bunsen-Ges.*, 1981, **85**, 863.
- P. D. I. Fletcher, A. M. Howe and B. H. Robinson, *J. Chem. Soc., Faraday Trans. 1*, 1987, **83**, 985–1006.
- J. Lang, A. Jada and A. Malliaris, *J. Phys. Chem.*, 1988, **92**, 1946–1953.
- A. D'Aprano, A. D'Arrigo, M. Goffredi, A. Paparelli and V. Turco Liveri, *J. Phys. Chem.*, 1989, **93**, 8367–8370.
- D. Bongiorno, L. Ceraulo, A. Ruggirello, V. Turco Liveri, E. Basso, R. Seraglia and P. Traldi, *J. Mass Spectrom.*, 2005, **40**, 1618–1625.
- G. Giorgi, L. Ceraulo and V. Turco Liveri, *J. Phys. Chem. B*, 2008, **112**, 1376–1382.
- B. Dereskei, A. Dereskei-Kovacs and Z. A. Schelly, *Langmuir*, 1999, **15**, 1981–1992.
- S. Abel, F. Sterpone, S. Bandyopadhyay and M. Marchi, *J. Phys. Chem. B*, 2004, **108**, 19458–19466.
- M. R. Harpham, B. M. Ladanyi and N. E. Levinger, *J. Phys. Chem. B*, 2005, **109**, 16891–16900.
- R. Allen, S. Bandyopadhyay and M. L. Klein, *Langmuir*, 2000, **16**, 10547–10552.
- D. W. Deamer and R. M. Pashley, *Origins Life Evol. Biosphere*, 1989, **19**, 21–38.
- J. Wang, R. M. Wolf, J. W. Caldwell, P. A. Kollman and D. A. Case, *J. Comput. Chem.*, 2004, **25**, 1157–1174.
- M. J. Frisch, G. W. Trucks, H. B. Schlegel, G. E. Scuseria, M. A. Robb, J. R. Cheeseman, J. A. Montgomery, Jr., T. Vreven, K. N. Kudin, J. C. Burant, J. M. Millam, S. S. Iyengar, J. Tomasi, V. Barone, B. Mennucci, M. Cossi, G. Scalmani, N. Rega, G. A. Petersson, H. Nakatsuji, M. Hada, M. Ehara, K. Toyota, R. Fukuda, J. Hasegawa, M. Ishida, T. Nakajima, Y. Honda, O. Kitao, H. Nakai, M. Klene, X. Li, J. E. Knox, H. P. Hratchian, J. B. Cross, C. Adamo, J. Jaramillo, R. Gomperts, R. E. Stratmann, O. Yazyev, A. J. Austin, R. Cammi, C. Pomelli, J. W. Ochterski, P. Y. Ayala, K. Morokuma, G. A. Voth, P. Salvador, J. J. Dannenberg, V. G. Zakrzewski, S. Dapprich, A. D. Daniels, M. C. Strain, O. Farkas, D. K. Malick, A. D. Rabuck, K. Raghavachari, J. B. Foresman, J. V. Ortiz, Q. Cui, A. G. Baboul, S. Clifford, J. Cioslowski, B. B. Stefanov, G. Liu, A. Liashenko, P. Piskorz, I. Komaromi, R. L. Martin, D. J. Fox, T. Keith, M. A. Al-Laham, C. Y. Peng, A. Nanayakkara, M. Challacombe, P. M. W. Gill, B. Johnson, W. Chen, M. W. Wong, C. Gonzalez and J. A. Pople, *GAUSSIAN 03 (Revision B.05)*, Gaussian, Inc., Pittsburgh, PA, 2003.
- C. I. Bayly, P. Cieplak, W. Cornell and P. A. Kollman, *J. Phys. Chem.*, 1993, **97**, 10269–10280.
- (a) D. A. Case, T. A. Darden, T. E. Cheatham III, C. L. Simmerling, J. Wang, R. E. Duke, R. Luo, M. Crowley, R. C. Walker, W. Zhang, K. M. Merz, B. Wang, S. Hayik, A. Roitberg, G. Seabra, I. Kolossvary, K. F. Wong, F. Paesani, J. Vanicek, X. Wu, S. R. Brozell, T. Steinbrecher, H. Gohlke, L. Yang, C. Tan, J. Mongan, V. Hornak, G. Cui, D. H. Mathews, M. G. Seetin, C. Sagui, V. Babin and P. A. Kollman, *AMBER 10*, University of California, San Francisco, 2008; (b) D. A. Case, T. E. Cheatham, III, T. Darden, H. Gohlke, R. Luo, K. M. Merz, Jr., A. Onufriev, C. Simmerling, B. Wang and R. Woods, *J. Comput. Chem.*, 2005, **26**, 1668–1688.
- T. Fox and P. A. Kollman, *J. Phys. Chem. B*, 1998, **102**, 8070–8079.
- M. P. Allen and T. J. Tildesley, *Computer Simulation of Liquid*, Clarendon Press, Oxford, 1987.
- J. Tsai, R. Taylor, C. Chothia and M. Gerstein, *J. Mol. Biol.*, 1999, **290**, 253–266.

-
- 20 F. Gangemi, G. Longhi, S. Abbate, F. Lebon, R. Cordone, G. P. Ghilardi and S. L. Fornili, *J. Phys. Chem. B*, 2008, **112**, 11896–11906.
- 21 W. Humphrey, A. Dalke and K. Schulten, *J. Mol. Graphics*, 1996, **14**, 33–38.
- 22 D. L. Bergman, L. Laaksonen and A. Laaksonen, *J. Mol. Graphics Modell.*, 1997, **15**, 301–306.
- 23 R. A. Sayle and E. J. Milner-White, *Trends Biochem. Sci.*, 1995, **20**, 374–376.
- 24 M. H. H. Pomata, D. Laria, M. S. Skaf and M. D. Elola, *J. Chem. Phys.*, 2008, **129**, 244503.
- 25 S. Havlin and D. Ben-Avraham, *Adv. Phys.*, 2002, **51**, 187–292.
- 26 A. Ruggirello and V. Turco Liveri, *Chem. Phys.*, 2003, **288**, 187–195.